Improved passive SAR imaging with DVB-T transmissions

Fang, Yue; Atkinson, George; Sayin, Alp; Chen, Jie; Wang, Pengbo; Antoniou, Michail; Cherniakov, Mike

DOI:
10.1109/TGRS.2020.2972156

License:
Other (please specify with Rights Statement)

Document Version
Peer reviewed version

Citation for published version (Harvard):
Fang, Y, Atkinson, G, Sayin, A, Chen, J, Wang, P, Antoniou, M & Cherniakov, M 2020, 'Improved passive SAR imaging with DVB-T transmissions', *IEEE Transactions on Geoscience and Remote Sensing*, pp. 1-11. https://doi.org/10.1109/TGRS.2020.2972156

Improved Passive SAR Imaging with DVB-T Transmissions

Yue Fang, George Atkinson, Alp Sayin, Jie Chen, *Senior Member, IEEE,* Pengbo Wang, *Member, IEEE,* Michail Antoniou, *Senior Member, IEEE,* Mikhail Cherniakov

***Abstract*—This paper investigates passive SAR image formation using Terrestrial Digital Video Broadcast (DVB-T) transmitters of opportunity and an airborne receiver. The proposed airborne system does not use separate channels for direct and reflected signal reception. The proposed image formation algorithm suppresses artefacts due to the presence of the direct signal in radar echo data using modified CLEAN method, and accounts for unknown irregularities in airborne platform motion using a map-drift autofocus (MDA) technique. The algorithms are theoretically derived and experimentally confirmed via an appropriate airborne campaign, and their experimental performance is measured.**

***Index Terms*— Passive SAR, DVB-T, SAR image formation, SAR autofocus.**

I. Introduction

Passive bistatic radar has been attracting much attention in the past few decades. In using non-cooperative illuminators of opportunity, such systems have several characteristic advantages compared to active radar, including cost effectiveness, silent operation, no need for frequency allocation and licensing, and a reduced footprint in terms of electro-magnetic pollution [1-3]. Many different types of available signals, including FM radio [4], Digital Audio Broadcast (DAB) [5], DVB-T [6], Global Navigation Satellite Systems (GNSS) [7], have been investigated for various applications, which include but are not limited to image formation, target location, moving target and coherent change detection.

In recent years, research on DVB-T passive SAR has been conducted with increasing interests. Despite the absence of global coverage and the modest resolution (8 MHz for a single DVB-T channel, giving a range resolution of 20m), this system is promising due to its very high transmit power (up to 100s' of kW), which enables imaging from large stand-off distances, and its low frequency (typically in the UHF band), which is generally known for its foliage penetration and indirect propagation effects.

The concept of DVB-T SAR has been experimentally shown by numerous systems created and flown independently by different groups around the world [8]-[17]. Most of these systems use separate channels for direct and reflected signal reception, with the direct signal being used to range compress radar data directly. In this paper, inspired by the Swedish LORA system (e.g. [12]), the direct signal channel is omitted. Apart from halving hardware complexity, there are several practical situations where this kind of configuration may be a desirable or even the only solution. For example, in the case of a spaceborne, rather than airborne receiver, it has been calculated that even a high-gain antenna (15 dB) onboard the satellite can inadvertently receive both the direct and reflected signals simultaneously from the antenna mainlobe [2]. Alternatively, if the passive radar is to be installed on small aircraft or even small drones, physically small, low-gain antennas should be used. But in this case, the main-to-backlobe ratio of the antenna reduces to the degree that the direct signal can be received from the backlobe almost as well as from its mainlobe (using small patch antennas the main-to-backlobe ratio can be as low as -3dB).

Apart from the tremendous potential the first experimental DVB-T SAR images have shown, they have also shown several artefacts that should be corrected moving forward. The problem of compensating for them using a single receiving channel additionally becomes more acute. The first set of artefacts arise from the presence of the direct signal in the radar data. Conventional methods for removing this signal in passive radar are based on CLEAN techniques [18-19], however those have not been extensively tested for passive SAR. Moreover, they rely on having a separate channel dedicated to recording the direct signal [20], which is not the case for the type of receiver this paper considers. The second set of artefacts arise in airborne systems due to unknown irregularities in platform motion. Those are generally corrected by autofocus routines, however those should be adopted and implemented for this kind of bistatic system and their performance on real data should be evaluated. Finally, potential problems due to the peculiarities of DVB-T waveforms, especially pilot signals whose effects are severe in passive radar, should be investigated to understand whether or not they should be specifically treated.

The goal of the paper is to derive an image formation algorithm for DVB-T SAR, which operates with single-channel data and accounts for the artefacts mentioned above to obtain

Manuscript received September 20, 2019. This work was supported by the National Science Foundation of China (NSFC) under Grant No. 61861136008, and the China Scholarship Council (CSC) under Grant No. 201806020022. The authors would like to thank Almat Aviation Ltd, for their support with airborne radar trials. (Corresponding author: Michail Antoniou).

Y. Fang, J. Chen and P. Wang are with the School of Electronic and Information Engineering, Beihang University, Beijing 100191, China (e-mail: fangyue@buaa.edu.cn; chenjie@buaa.edu.cn; wangpb7966@buaa.edu.cn).

G. Atkinson, M. Antoniou and M. Cherniakov are with the Department of Electronic, Electrical and Systems Engineering, University of Birmingham, Birmingham B15 2TT, U.K. (e-mail: gma241@student.bham.ac.uk; m.antoniou@bham.ac.uk; m.cherniakov@bham.ac.uk).

A. Sayin was with the Microwave Integrated Systems Laboratory of University of Birmingham, Birmingham, B15 2TT, U.K. He is now with Novit.AI, METU Technopark Ankara, 06800, TURKEY (e-mail: alpsayin@alpsayin.com).

improved DVB-T SAR imagery. Specifically, the algorithm is theoretically derived assuming DVB-T waveforms, which allows an investigation on effects of pilot signals. A modified CLEAN technique is developed to suppress direct signal returns using a single receiving channel. Finally, a basic Map-Drift Autofocus (MDA) is adopted for DVB-T SAR. The validity and performance of the algorithm is measured through airborne experimental data.

The rest of the paper is organized as follows: In Section II, the geometry of airborne passive bistatic SAR is firstly presented, and the detailed signal processing flows of airborne passive SAR with autofocusing using DVB-T signals are presented, including the range compression and effects analyses of pilot signals on image formation, direct signal suppression using the modified CLEAN method, back-projection algorithm (BPA) using single receive channel, and autofocus processing using the MDA algorithm. Section III shows the experiment processing results of airborne passive SAR using DVB-T signals. Finally, conclusions are drawn in Section IV.

II. Signal Processing Algorithm

A simplified geometric configuration of airborne passive bistatic SAR is shown in Fig. 1. Here, a DVB-T signal transmitter is used as the illuminator of opportunity, and a receiver is mounted on an airplane with velocity of V, whose distance from the transmitter is L. The movement of the aircraft during the integration time T_d forms the synthetic aperture.

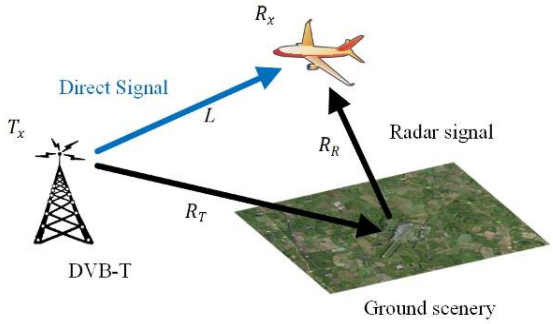

Fig. 1. Geometry structure of airborne passive SAR.

A block diagram showing the major steps of the algorithm is presented in Fig. 2. The first part of the algorithm is range compression (RC). Regardless of the number of receiving channels, the presence of the direct signal in the radar data will result in compressed direct signal returns whose intensity will be high. The second part of process followed is the direct signal suppression (DSS). The CLEAN method is utilized after the range compression to remove the direct signal in the range compressed radar signal. The complex image matrix correlation coefficient of the compressed direct signal and the radar signal is calculated in the time domain. Then, BPA is performed to achieve the cross-range compression, combined with the motion information acquired from the IMU and the GPS. The final part denotes the image autofocus processing. A Map-drift autofocus (MDA) algorithm is applied on the focused image after the BP image formation. The details of each part are presented in the following subsections.

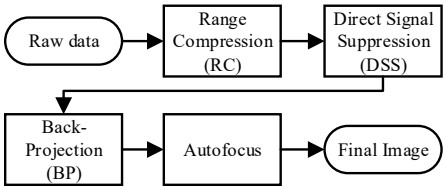

Fig. 2. Flowchart of the whole signal processing.

A. RC processing

In a single-channel receiver, containing both the direct and reflected signals, RC can be obtained by auto-correlating the recorded radar data in the channel [6], [15]. As DVB-T transmits continuously, an equivalent Pulse Repetition Frequency (PRF) can be chosen as that of a DVB-T symbol, which for our case is 1082.3Hz.

At the same time, due to the specific structure of the DVB-T signals, modulated using the Orthogonal Frequency Division Multiplexing (OFDM), there are additional pilot carriers existing in the direct and echo signals, whose effects on imagery should be investigated. Many researchers have focused on the ambiguity function (AF) of DVB-T signals [21]-[23], and therefore the position of the pilots after range compression can be derived according to the zero Doppler profile of AF.

Firstly, the baseband structure of the DVB-T signals is expressed as follows [24],

$$x(t)=\sum_{m=0}^{\infty}\sum_{l=0}^{L-1}\sum_{k=0}^{K-1}c_{mlk}e^{j2\pi\frac{k}{T_U}(t-T_U-lT_S-mLT_S)}\cdot w(t-lT_S-mLT_S) \quad (1)$$

where the meanings of every variable in Eq. (1) are listed in Table I.

Table I
VARIABLE DEFINITION

Variable	Meaning
m	OFDM frame number
l	OFDM symbol number
k	Carrier number
c_{mlk}	Complex value coefficients
T_U	Duration of useful part
T_S	Symbol duration
L	Symbol number
K	Carriers number
$w(\cdot)$	Rectangular window

Ignoring the amplitude terms of Eq. (1), the direct signal recorded in the receive channel is given by

$$d(t)=x(t-\tau_0) \quad (2)$$

where $\tau_0=\frac{L}{c}$, and L denotes the range between transmitter and receiver.

Similarly, the reflected signal from a single point target recorded in the receive channel is written as

$$r(t)=x(t-\tau_1) \quad (3)$$

where $\tau_1 = \frac{R_T + R_R}{c}$; R_T represents the range between transmitter and target, and R_R represents the range between receiver and target.

In our DVB-T system with a single receiving channel, both the direct signal and the reflected signal are included in the echo data, and the surveillance signal can be represented as,

$$s(t) = A_d d(t) + A_r r(t) \tag{4}$$

where A_d and A_r represent the amplitude components of the direct signal and reflected signal, respectively.

Then, range compression is finished by the auto-correlation of surveillance signal, shown as follows,

$$\mathrm{sc}(\tau) = \int_{-\infty}^{\infty} s(t) \cdot s^*(t-\tau)\, dt \tag{5}$$

R2-3 where * denotes the complex conjugate.

Substituting Eq. (2-4) to Eq. (5), and ignoring the amplitude coeffcients, the correlated signal can be derived as,

$$\mathrm{sc}(\tau) = R_d(\tau) + R_r(\tau) + R_{dr}(\tau) + R_{rd}(\tau) \tag{6}$$

In Eq. (6), the first and second terms represent the auto-correlation function of pure direct signal and reflected signal. The third and fourth items include the targets information.

Hence, the third item in Eq. (6) is shown as,

$$R_{dr}(\tau) = \int_{-\infty}^{\infty} d(t) \cdot r^*(t-\tau)\, dt \tag{7}$$

Substitute $r(t)$ and $\mathrm{s}(t)$ into $sc(\tau)$.

$$R_{dr}(\tau) = \int_{-\infty}^{\infty} x(t-\tau_0) \cdot x^*(t-\tau_1-\tau)\, dt \tag{8}$$

Replace $t-\tau_0 = t$,

$$R_{dr}(\tau) = \int_{-\infty}^{\infty} x(t) \cdot x^*(t-\Delta-\tau)\, dt \tag{9}$$

where $\Delta = \tau_1 - \tau_0 = \frac{R_T + R_R - L}{c}$.

Compare with the derivation of the ambiguity function [21-23], that is,

$$AF(\tau, v) = \int_{-\infty}^{\infty} d(t) \cdot r^*(t-\tau) e^{-j2\pi vt}\, dt \tag{10}$$

$R_{dr}(\tau)$ can be represented as $R_{dr}(\tau) = AF(\tau + \Delta, 0)$. Similarly, $R_{rd}(\tau)$ can be derived as $R_{rd}(\tau) = AF(\tau - \Delta, 0)$.

The location of range-compressed pilot signals within one symbol duration will be located in [23],

$$\tau = \Delta \pm \left\{0, \frac{k}{12} T_U, T_S\right\}, k = 1, 2, \ldots, 12 \tag{11}$$

Eq. (11) shows that after range compression, there are ambiguous peaks due to the presence of pilot signals, which are separated in time by $kT_U/12$. Because pilot locations are constant in each DVB-T symbol, we may then expect that the ambiguous range-compressed peaks will result in ambiguous range histories every $kT_U/12$ s (Fig. 3).

However, it can be found that after image formation these ambiguities may be largely suppressed, for a number of reasons. Firstly, for a single DVB-T symbol, the amplitude of the ambiguities is nearly 20dB below the main peak, however the direct signal could be 46-60dB stronger than the reflected signal. More importantly, this is further attenuated by the operation of the image formation algorithm as a spatial filter. As an example, consider the first ambiguity, occurring at $kT_U/12$ s. For $T_u = 896\mu s$, and a quasi-monostatic acquisition, this corresponds to a round-trip distance of about $\Delta \pm 22.4$ km, but its range and phase history will be related to Δ only. This means that the phase of the BPA filter at that location will be mismatched to that of the ambiguity, resulting in further suppression, and the mismatch will be progressively worse for pilot peaks beyond the first (Fig. 3).

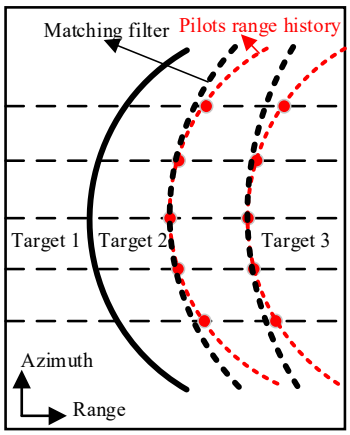

Fig. 3. Pilots range history illustration.

The phase difference results from the mismatch between target 2 and the pilot, and the quadratic phase error (QPE) can be calculated according to the second order phase difference after the range compression. To calculate the degree of suppression, a simple case may be considered.

For the quasi-monostatic airborne passive SAR, the QPE can be acquired by Eq. (12), shown as follows,

$$\varphi_{QPE} = e^{-j\frac{4\pi}{\lambda}\left[\frac{V^2}{2}\left(\frac{1}{\Delta} - \frac{1}{\Delta + r_{pilots}}\right)\left(\frac{T_s}{2}\right)^2\right]} \tag{12}$$

where λ is the wavelength, and V denotes the aircraft velocity. r_{pilots} represents the pilots' position. T_s is the aperture time.

Fig. 4 shows the QPE values in different nearest slant range Δ with different aperture time, centred at the frequency 650MHz, where V is 240km/h.

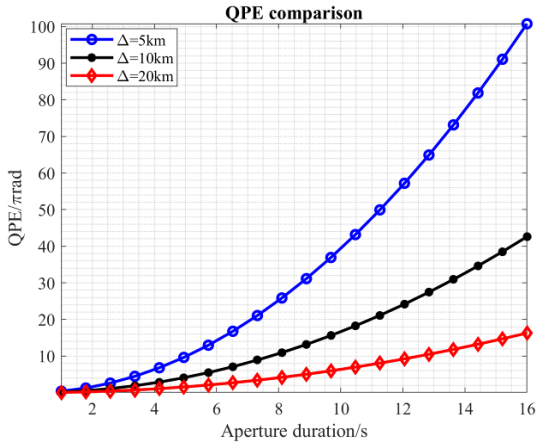

Fig. 4. QPE analysis via aperture durations in different nearest slant range Δ.

It can be seen that QPE is far higher than required typical threshold $\pi/4$, where the target will defocus seriously. Fig. 5 gives the results of simulated azimuth signals with matched filtering and mismatched filtering in terms of $\Delta = 5\text{km}$, and $T_s = 16\text{s}$. The amplitude of pilots is suppressed below -25dB, which is far lower than the first side-lobe of the actual target in this position.

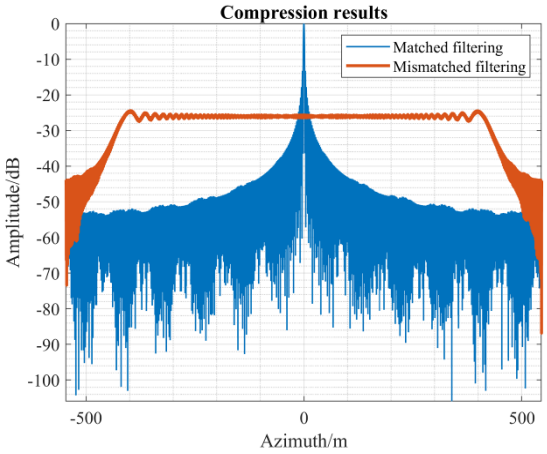

Fig. 5. Azimuth compression results with matched filtering and mismatched filtering.

That is, pilots will be suppressed after azimuth compression effectively. And as a result, the influence of pilots can be negligible in terms of imaging performance.

The implication of this finding is that while complex DVB-T direct signal decoding and re-modulation (e.g. [25]) algorithms may be an essential part for passive surveillance radar using DVB-T to compensate for ambiguities due to pilots, they may not be necessary (although optimal) for DVB-T SAR purposes. In this case, a substantially reduced algorithm complexity would be achieved, especially taking into account Doppler spread on OFDM due to SAR platform motion [26], at the cost of a sub-optimal performance which requires a dedicated study beyond the scope of this paper.

B. DSS processing

A standard method to suppress the direct signal in passive/bistatic radar data is based on CLEAN techniques. However, these techniques are not directly applicable to the system proposed here, because they either assume the transmitted signal is known, or a dedicated channel is used for direct signal reception (an example such method for bistatic SAR is in [20]), or both.

In a single receiving channel, the direct and reflected DVB-T signals co-exist, and therefore a modified CLEAN technique should be derived to obtain the reference direct signal needed for CLEAN to operate. The proposed algorithm is a modification of the algorithm in [20] to overcome these problems, and its block diagram is shown in Fig. 6. The method mainly includes three parts, feature extraction (red dash line), matrix correlation coefficient calculation (blue dash line) and image subtraction (purple dash line).

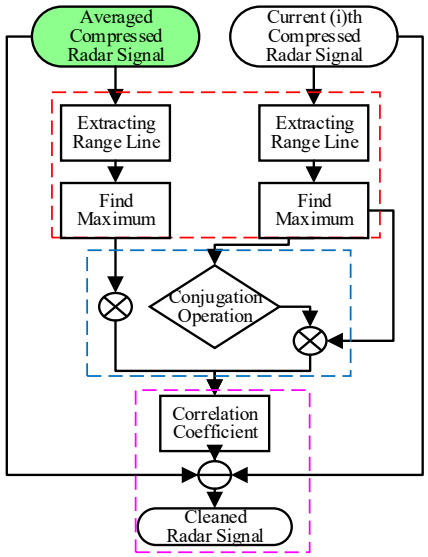

Fig. 6. Flowchart of DSS.

The algorithm adopts a progressive mean method to obtain the reference signal, shown in the green rounded rectangle Fig. 6. An estimate of the reference signal for a given aperture position, or azimuth sample, (indicated by a green arrow) is provided by averaging signals recorded over a set of previous SAR aperture positions (where the length of data recorded is equal to one DVB-T symbol). The idea is that over a limited amount of time, the direct signal may remain largely unchanged, but complex reflected echoes from the target area may not, and this effect may be more prominent after averaging.

R3-1

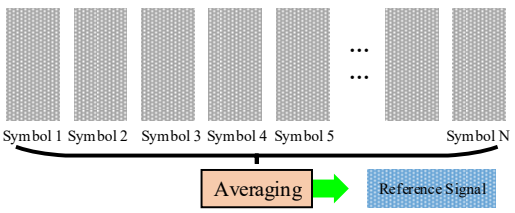

Fig. 7. The illustration of progressive mean method.

Firstly, each range line from the current compressed radar signal and previous compressed radar signals need to be extracted, $sc_r(i,:)$ and $sc_d(i,:)$, where i is the current symbol index, and the second dimension represents this whole range line data. The index of maximum amplitudes Jr_{max} and Jd_{max} should be acquired. The number of symbols used for reconstructing the reference signal is N, shown in Fig. 7, and it is relative to the performance of the direct signal cancellation. Here, in the processing part, the N value equals to N_a.

Then, the matrix correlation coefficient is calculated using Eq. (13),

$$C_{mcc} = \frac{\sum_{i=1}^{N_a} sc_d^*(i, Jd_{max}) \cdot sc_r(i, Jr_{max})}{\sum_{i=1}^{N_a} sc_r^*(i, Jr_{max}) \cdot sc_r(i, Jr_{max})} \tag{13}$$

where N_a represents the number of DVB-T symbols, or receiver azimuth positions, over the whole dwell time.

Finally, image matrix subtraction is followed by using Eq. (14),

$$sc_{cleaned}(i,j) = sc_r(i,j) - C_{mcc} \cdot sc_d(i,j) \tag{14}$$

where i and j are the azimuth index and range index, respectively. In this way, the direct signal may be suppressed without prior knowledge of the direct signal waveform, or a need to use a dedicated channel to measure it.

C. BPA processing

BPA is finally utilized to compress echoes in azimuth, as it is suitable and straightforward to implement for the complexity imaging geometry of passive SAR. The algorithm is standard and well-known, however it is mentioned very briefly here for the sake of completion.

Firstly, three slant ranges need to be calculated in bi-static radar, including R_{ts}, R_{rs} and R_{tr}, which represent range between transmitter and scene, receiver and scene, and transmitter and receiver, respectively. The corresponding time delay can be obtained by,

$$t_{delay} = \frac{R_{ts} + R_{rs} - R_{tr}}{c} \tag{15}$$

Then, the phase item used in BPA is acquired by

$$\Phi_{BPA} = \exp\{j2\pi f_c t_{delay}\} \tag{16}$$

where f_c represents the system carrier frequency.

In order to find the accurate signal amplitude and phase at a certain range, interpolation is necessary in each range line. Finally, image reconstruction can be achieved by phase multiplication, shown in (17).

$$s_{image} = \sum_{i_a=1}^{N_a} s_{cleaned} \cdot \Phi_{BPA} \tag{17}$$

where N_a denotes the pulses number in the BPA accumulation.

D. Autofocus processing

Due to the unstable flight of an airborne platform, motion error seriously affects image formation focusing performance,. Although the IMU/GPS is considered in the system operation to record real-time position and velocity information, it is not accurate enough to fulfil the image performance requirements. Image autofocus processing is a way of addressing this issue. In this section, a traditional MDA [27] has been modified for passive airborne SAR. The flowchart of the MDA algorithm is illustrated in Fig. 8. Of course more complex algorithms such as Phase Gradient (PG) [28] can fundamentally be adopted. However, an MDA implementation is simpler, and even more so in bistatic systems since the directions of the range and azimuth sidelobes and spatial resolutions are no longer orthogonal [29, 30], which can create additional complications for PG-type algorithms. The MDA is more resilient to such effects since its processing is mainly performed in the data, rather than image domain.

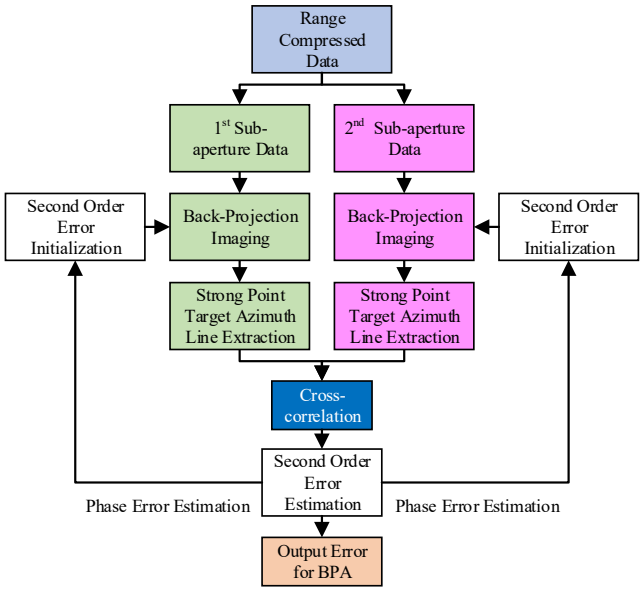

Fig. 8. Flowchart of the modified MDA for BPA

Second-order phase errors are assumed in the azimuth direction within the whole aperture time. If the echo data are separated into two sub-apertures, there will be a linear component in each sub-aperture, which will lead to an image drift in the final image. MDA calculates the second order phase error by the cross-correlation of these two sub-images, and iterates this process for the better estimation of the phase error.

It is noted here that the MDA is traditionally applied to frequency-based imaging algorithms, where there is a mapping relation for second-order phase errors between the image domain and the aperture domain. However, since the BPA is based on signal processing in the time domain, it is more complex to determine this mapping relation. Therefore, the first initial value of the second order phase error is difficult to be acquired accurately and requires more iterations.

Firstly, it can be assumed that phase error is denoted by $\varphi(t) = exp\{j\pi bt^2\}$, and linear item after sub-aperture

operation can be produced as $k_L = \pi b T_a$, where $T_a = N_a / PRF$ represents the azimuth dwell time. This linear item will introduce the image drift, corresponding to a frequency shift as $k_L / 2\pi = bN_a / 2PRF$, which equals to $bN_a^2 / 2PRF^2$. Hence b can be derived according to the linear item in the sub-aperture of the $\varphi(t)$, expressed as,

$$b = 2N_{drift}\left(\frac{PRF}{N_a}\right)^2 \tag{18}$$

where N_{drift} is the image drift amount, PRF denotes the pulse repetition frequency, and N_a is the azimuth sampling numbers in the whole aperture.

After calculating the b parameter, the initial phase error $\varphi(t)$ can be constructed and adopted in BPA processing. Then, two new sub-aperture images can be generated, which will be used for the next estimation of the phase error.

Due to the fact that complex mapping relation between time domain and image domain of BPA, we simplify Eq. (18) and use the amount acquired in the current imaging grids, and acquire final accurate phase error by iteration.

Then the estimated phase error is iterated into a new loop for the next iteration of phase error estimation, and the processing stops at a point where the sub-images drift amount can be negligible.

III. Experimental Results

In this section, an airborne experimental campaign is described. The DVB-T transmitter used was the Sutton Coldfield broadcasting station in the UK, which was mounted on a 264m tall mast on the top of a hill. The airborne platform was a 4-seat Cessna 172N Skyhawk aircraft, and the receiving antenna was placed on the side of the aircraft, pointing towards the target area, with measured beamwidths of 50˚ with gain of about 9 dB, and the forward-back lobe ratio of the antenna used was around 3 dB. The GPS antenna of the IMU was installed at the back of the plane, where its distance from the radar antenna was considered in the image formation.

The experiments were conducted at an aircraft altitude of 600m above mean sea level, with an average ground speed at 240 km/h, and the echo signals were collected by recording a single DVB-T channel, where the centre frequency was 650MHz. Table II shows the experimental parameters.

Table II
Experimental Parameters

Property	Value	Unit
Carrier frequency	650	MHz
Transmit power	200	kW
Transmitter mast height	264	m
Transmitter grazing angle	0.5	°
Rx antenna beamwidth	50	°
Bandwidth	7.6	MHz
Dwell time	8, 16	s
Average ground speed	240	km/h
Aircraft altitude	600	m

Different dwell times (8s and 16s) were tested with slightly varying geometries (approaching quasi-monostatic) at two different sites. The goal was then to illustrate the feasibility and measure the performance of DSS and autofocus processing. For DSS validation, the target area was around Stoke Golding (23.4km from the transmitter), with a dwell time of 8s, since the direct signal was pronounced in imagery. The second target area was the Bruntingthorpe Aerodrome, (43.4km from the transmitter), with a dwell time of 16s to verify autofocus, since in that target area bright point-like scatterers were found for evaluation. Strong single point-like targets extracted from the image results were analysed by two dimensional cross section profiles and 3dB resolution.

A. CLEAN results

In the validation experiment of the CLEAN method, the imaging geometry we used here is shown in Fig. 9. The distance from the transmitter to the receiver aperture centre is about 23.4km. The flight path and the imaging area are marked in the figure.

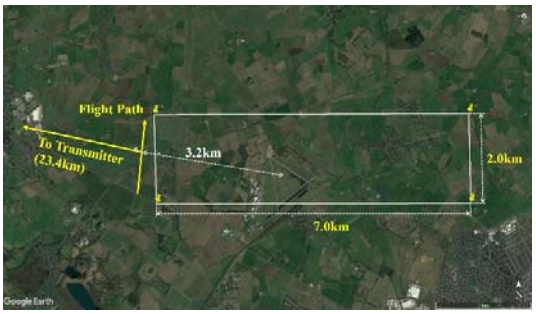

Fig.9. Experiment scenario of CLEAN method validation.

The comparison between the original results and cleaned results are shown in Fig. 10(a-b), and an optical satellite image is shown in Fig. 10(c) for comparison. Comparing Fig. 10(a) and Fig. 10(c), the horizontal bright in Fig. 10(a) lines are the direct signal component, rather than the real area information, while this direct signal component has been suppressed obviously in Fig. 10(b), while target information is retained.

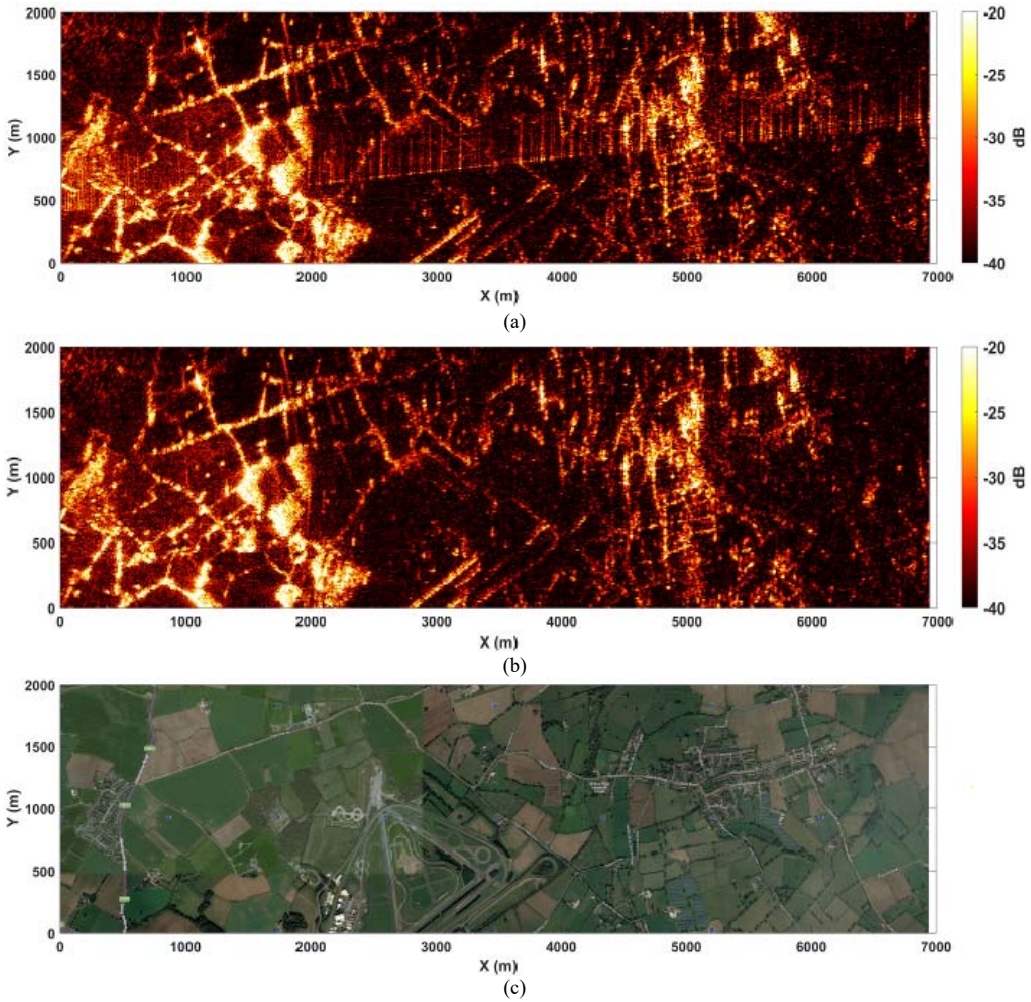

Fig.10. Imaging results of 8s aperture time: (a) Original image, (b) cleaned image, and (c) Satellite image (Bing Maps).

In order to evaluate further influences of the CLEAN method, the image contrast, dynamic range of the image results have been analyzed. Table III gives the image analyses in Fig. 10.

TABLE III
IMAGE ANALYSES

Index	Origin	Clean
Image Contrast/dB	71.066	71.056
Dynamic Range/dB	107.251	113.500

R3-1

According to the image analyses comparison results, the image dynamic range, which represents the ratio of the maximum and minimum amplitude value, has been enhanced from 107.251 dB to 113.500 dB, about 6 dB improvement. At the same time, image contrast is not corrupted by the proposed method, nearly keeping the same compared with those of the original image.

From the results and analyses above, the proposed modified CLEAN method can be used for DSS, and direct signal can be removed effectively. Image dynamic range can be enhanced after the CLEAN processing.

B. *Autofocus results*

For the purpose of confirming the effectiveness of the proposed MDA algorithm, experiment data with 16s dwell time have been tested. For the iteration criterion in this experimental processing, the iteration was set to be stopped when the changing percent of coefficient b was lower than 0.1 percent compared with the last round of iteration. About 9240 range lines were utilized to generate the sub-images during the MDA processing, with the phase error estimated by observing and calculating the images drift amount.

R3-2

The imaging geometry used is shown in Fig. 11. The distance from the transmitter to the receiver aperture centre was about 43.4km, and the imaging area around the Bruntingthorpe Aerodrome is selected, near Leicester, UK. The aerodrome is about 5.5km away from the receive aperture centre, and the imaging area is about $10.0\text{km}\times 6.7\text{km}$.

R1-3

Fig. 11. Experiment scenario of autofocus algorithm validation.

Fig. 12 shows a comparison between the original results and autofocused results of 16s aperture time after the MDA algorithm, where the second image (Fig. 12(b)) is the results using the MDA method, and the CLEAN method is also applied together.

Three point-like targets for evaluation are selected from the image results shown in Fig. 13. The first target is located at (9183m, -1367m), the position of the second one is (8675m, -1463m), and the third one is (8803m, 64.82m) in the original images.

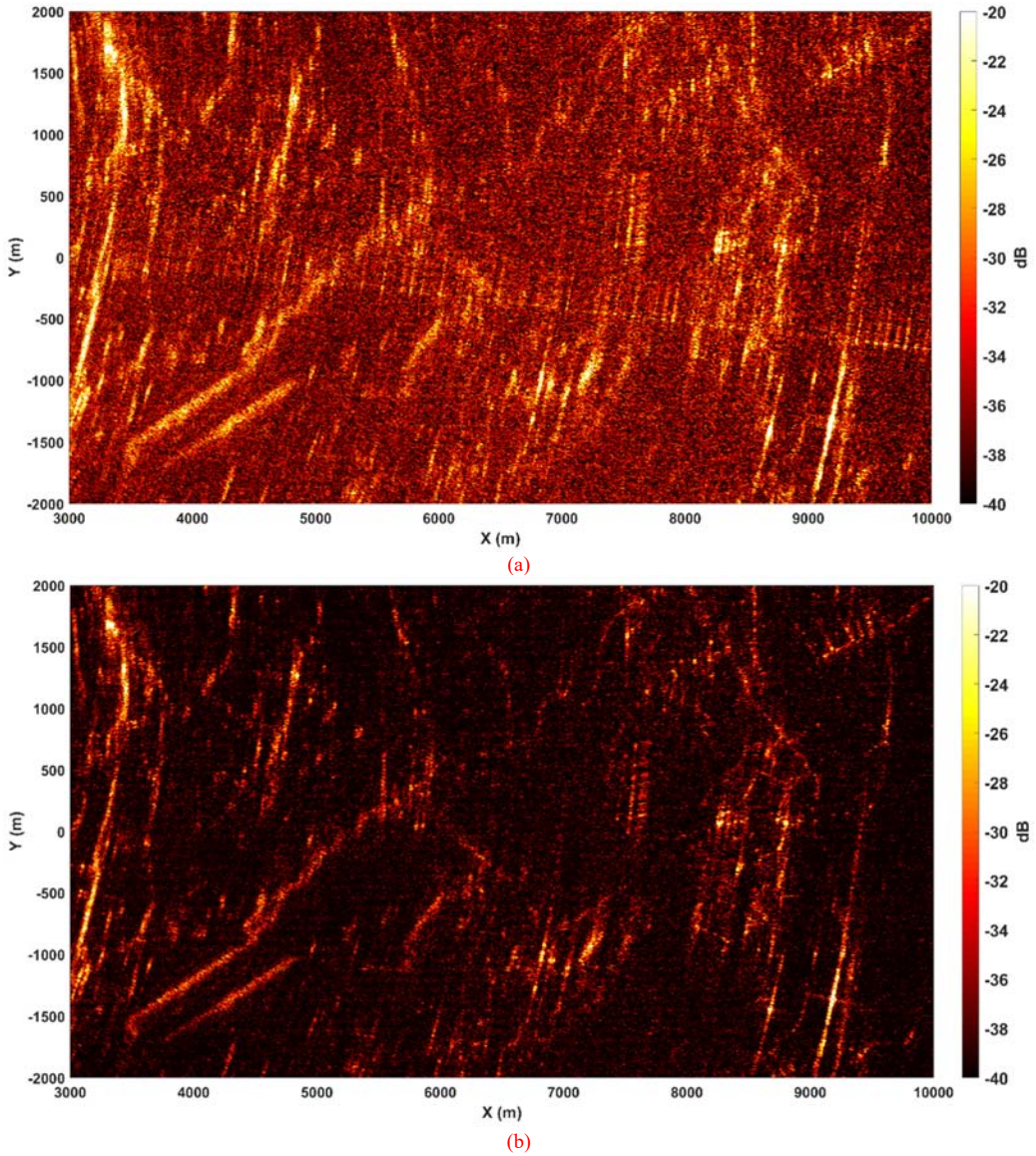

R1-3

Fig. 12. Autofocus results of 16s aperture time: (a) Original image, (b) autofocused image.

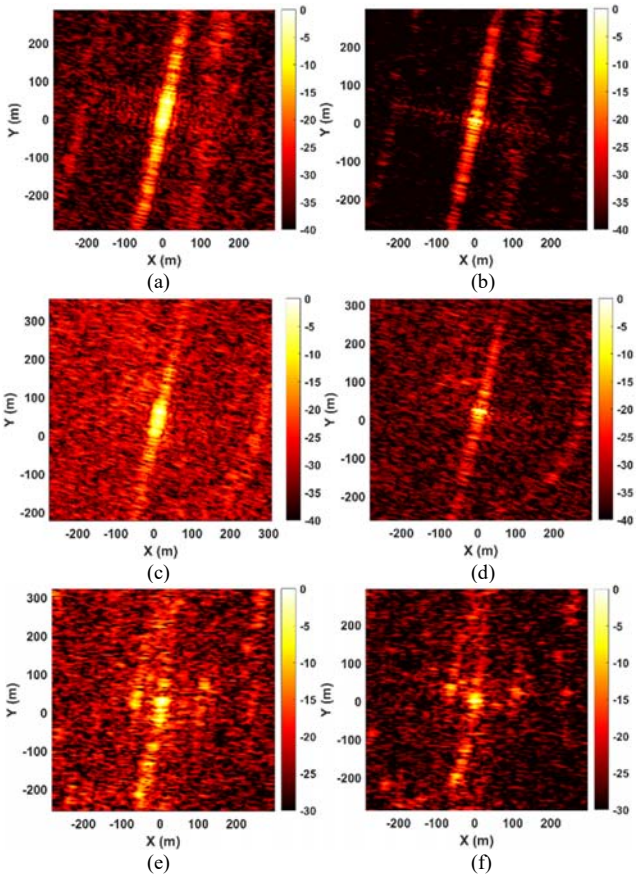

Fig. 13. Extracted PSF of three point-like targets for the 16s aperture dwell time. (a, c, e,) Original image, (b, d, f) autofocused image.

According to Fig. 13(b, d, f), the three targets have been well compressed after our autofocus, and the area of targets main-lobe section has deduced. Fig. 14 gives the 2-dimensional profiles of three point-like targets. As for profiles in the range direction, the main-lobe after autofocus remains the same while side-lobes have decreased. It is also seen that the profiles in the cross-range direction have been remarkably improved. The cross-range resolution has improved, while the side-lobes of these targets have decreased significantly. The point targets azimuth evaluation results of Fig. 14 are summarized in Table IV.

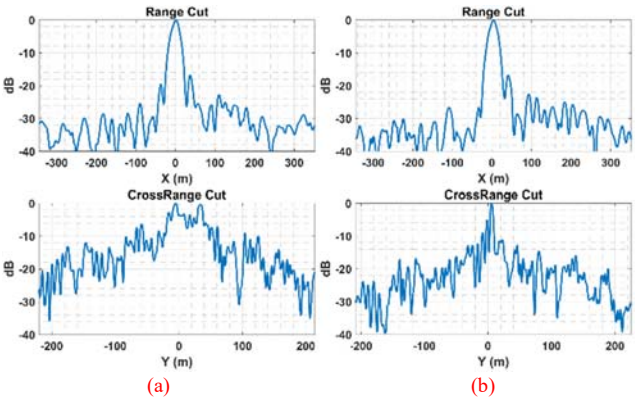

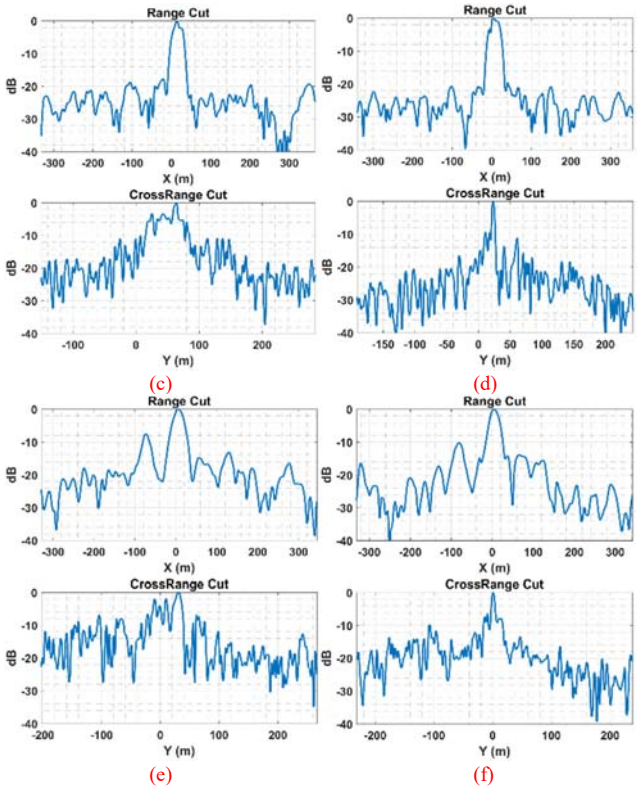

Fig. 14. Cross-Sections of extracted PSF from three point-like target for the 8s aperture time. (a, c, e) Original image, (b, d, f) autofocused image.

Table IV
CROSS-RANGE RESOLUTION EVALUATION

Resolution Evaluation	Original	Autofocus	Theoretical Value
Point Target 1	7.399 m	3.806 m	3.625
Point Target 2	6.757 m	3.404 m	3.344
Point Target 3	14.037 m	5.521 m	3.694

R3-2

From Fig. 12-14 and Table IV, after autofocus processing, the image dynamic range has increased about 3dB, from 109.9dB to 112.1dB, and the image contrast has improved about 0.1dB, from 73.50dB to 73.59dB. The peak power of the image has enhanced 1.7dB, from 74.81dB to 76.53dB, and the peak power of these three targets has increased about 0.2dB, 1.4dB and 0.3dB, respectively. The azimuth resolution has significantly improved adequately. At the same time, the azimuth sidelobes have been suppressed.

R3-2

Thus, it can be concluded that these imaging and evaluation results confirm the effectiveness of the MDA method, and the azimuth phase error estimation ability is also validated, especially in terms of the quadratic phase error, which influence the azimuth focusing performance.

IV. CONCLUSION

In this paper, an improved airborne passive SAR image formation with DVB-T transmitters of opportunity using one receive channel has been presented. A DSS algorithm was proposed using a modified CLEAN method with progressive means along the aperture, and airborne platform motion errors were considered using a MDA technique.

The algorithms were verified through experimental airborne

data. It was shown that after DSS processing, the direct signal mixed in the radar signal was removed effectively. The dynamic range of the image after CLEAN was enhanced. The focusing performance was improved using MDA algorithm. Selected point-like targets were evaluated, and 2-dimensional profiles showed a better cross-range resolution and decreased side-lobes.

REFERENCES

[1] M. Cherniakov, Bistatic radar: emerging technology: John Wiley & Sons, 2008.

[2] M. Antoniou, A. G. Stove, A. Sayin, G. Atkinson, M. Cherniakov, H. Ma, H. Kuschel, D. Cristallini, P. Wojaczek, and C. I. Underwood, "Passive SAR satellite constellation for near-persistent earth observation: Prospects and issues," *IEEE Aerosp. Electron. Syst. Magazine*, vol. 33, no. 12, pp. 4-15, 2018.

[3] H. D. Griffiths, and C. J. Baker, An introduction to passive radar: Artech House, 2017.

[4] F. Colone, D. O'hagan, P. Lombardo, and C. Baker, "A multistage processing algorithm for disturbance removal and target detection in passive bistatic radar," *IEEE Trans. Aerosp. Electron. Syst.*, vol. 45, no. 2, pp. 698-722, 2009.

[5] C. Coleman, and H. Yardley, "Passive bistatic radar based on target illuminations by digital audio broadcasting," *IET Radar, Sonar & Navigation*, vol. 2, no. 5, pp. 366-375, 2008.

[6] G. Atkinson, A. Sayin, A. Stove, C. I. Underwood, M. Cherniakov, and M. Antoniou, "Passive SAR satellite (PASSAT) system: airborne demonstrator and first results," *IET Radar, Sonar & Navigation*, vol. 13, no. 2, pp. 236-242, 2018.

[7] M. Antoniou, and M. Cherniakov, "GNSS-based bistatic SAR: A signal processing view," *EURASIP Journal on Advances in Signal Processing*, vol. 2013, no. 1, pp. 98, 2013.

[8] D. Gromek, P. Krysik, K. Kulpa, P. Samczyński, and M. Malanowski, "Ground-based mobile passive imagery based on a DVB-T signal of opportunity," *in Proc. IEEE RadarCon*, Oct. 13-17, 2014, pp. 1-4.

[9] D. Gromek, P. Samczyński, K. Kulpa, P. Krysik, and M. Malanowski, "Initial results of passive SAR imaging using a DVB-T based airborne radar receiver," *in Proc. IEEE 11th EuRAD*, Oct. 8–10, 2014, pp. 137-140.

[10] D. Gromek, K. Kulpa, and P. Samczyński, "Experimental results of passive SAR imaging using DVB-T illuminators of opportunity," *IEEE Geoscience and Remote Sensing Letters*, vol. 13, no. 8, pp. 1124-1128, 2016.

[11] D. Gromek, K. Radecki, J. Drozdowicz, P. Samczyński and J. Szabatin, "Passive SAR imaging using DVB-T illumination for airborne applications," *IET Radar, Sonar & Navigation*, vol. 13, no. 2, pp. 213-221, 2019.

[12] L. M. Ulander, P.-O. Frölind, A. Gustavsson, R. Ragnarsson, and G. Stenström, "VHF/UHF bistatic and passive SAR ground imaging," *in Proc. IEEE RadarCon*, May 10-15, 2015, pp. 0669–0673.

[13] L. M. Ulander, P.-O. Frölind, A. Gustavsson, R. Ragnarsson, and G. Stenström, "Airborne passive sar imaging based on dvb-t signals," *in Proc. IEEE Int. Conf. Geosci. Remote Sens. Symp.*, 2017, pp. 2408-2411.

[14] P.-O. Frölind, "Results of airborne passive SAR ground and sea target imaging using DVB-T signals." *in Proc. IEEE RadarCon*, May 2-6, 2016, pp. 1-4.

[15] P.-O. Frölind, A. Gustavsson, A. Haglund, R. Ragnarsson, and L. M. Ulander, "Analysis of a ground target deployment in an airborne passive SAR experiment," *in Proc. IEEE RadarCon*, May 8-12, 2017, pp. 0273-0278.

[16] G. Atkinson, A. Sayin, C. Underwood, M. Cherniakov, and M. Antoniou, "Passive SAR Satellite System (PASSAT): Ground Trials," *in Proc. IEEE Int. Conf. Radar*, Aug. 27-31, 2018, pp. 1-6.

[17] I. Walterscheid, P. Wojaczek, D. Cristallini, and A. Summers, "Challenges and first results of an airborne passive SAR experiment using a DVB-T transmitter," *in EUSAR 2018; 12th European Conf. on Synthetic Aperture Radar*, Jun. 4-7, 2018, pp. 1-4.

[18] K. Kulpa, "The CLEAN type algorithms for radar signal processing," *in Proc. Symp. MRRS*, Sep. 2008, pp. 152–157.

[19] J. L. Garry, C. J. Baker, and G. E. Smith, "Evaluation of direct signal suppression for passive radar," *IEEE Trans. Geosci. Remote Sens.*, vol. 55, no. 7, pp. 3786–3799, 2017.

[20] K. Kulpa, P. Samczynski, M.Malanowski, L.Maslikowski, and V. Kubica, "The use of CLEAN processing for passive SAR image creation," in *Proc. IEEE RADAR*, Apr. 29–May 3, 2013, pp. 1–6.

[21] R. Saini and M. Cherniakov, "DTV signal ambiguity function analysis for radar application," *Proc. Inst. Electr. Eng.—Radar Sonar Navig.*, vol. 152, pp. 133–142, Jun. 2005.

[22] F. Colone, D. Langellotti, P. Lombardo, "DVB-T signal ambiguity function control for passive radars", *IEEE Trans. Aerosp. Electron. Syst.*, vol. 50, no. 1, Jan. 2014.

[23] J. E. Palmer, H. A. Harms, S. J. Searle, L. M. Davis, "DVB-T passive radar signal processing", *IEEE Trans. Signal Process.*, vol. 61, no. 8, pp. 2116-2126, Apr. 2013.

[24] Digital Video Broadcasting (DVB); Framing Structure, Channel Coding and Modulation for Digital Terrestrial Television (DVB-T). *European Telecommunications Standards Institute*, Mar. 1997.

[25] H. Kuschel, M. Ummenhofer, D. O'Hagan and J. Heckenbach, "On the resolution performance of passive radar using DVB-T illuminations," *in Proceedings of the 11th International Radar Symposium*, Vilnius, Lithuania, 2010, 1–4.

[26] C. Berthillot, A. Santori, O. Rabaste, D. Poullin and M. Lesturgie, "BEM reference signal estimation for an airborne passive radar antenna array", *IEEE Trans. Aerosp. Electron. Syst.*, vol. 53, no. 6, Dec, 2017, pp. 2833-2845.

[27] C. V. Jakowatz, D. E. Wahl, P. H. Eichel, D. C. Ghiglia, and P. A. Thopson, Spotlight-Mode Synthetic Aperture Radar: A Signal Processing Approach. Berlin, Germany: Springer, 1996.

[28] D. E. Wahl, P. H. Eichel, D. C. Ghiglia, and C. V. Jakowatz, Jr, "Phase gradient autofocus-a robust tool for high resolution SAR phase correction," *IEEE Trans. Aerosp. Electron. Syst.*, vol. 30, no. 3, pp. 827–835, Jul. 1994.

[29] T. Zeng, M. Cherniakov, and T. Long, "Generalized approach to resolution analysis in BSAR," *IEEE Trans. Aerosp. Electron. Syst.*, vol. 41, no. 2, pp. 461–474, Apr. 2005.

[30] F. Santi, M. Antoniou, and D. Pastina, "Point spread function analysis for GNSS-based multistatic SAR," *IEEE Geosci. Remote Sens. Lett.*, vol. 12, no. 2, pp. 304–308, Feb. 2015.